Modeling and Analysis of a Gas Sweeping Process for Polycarbonate Polymerization

Dae-Hyung Kim,[1] Kyoung-Su Ha,[1] Hyun-Ku Rhee,[1] Kwang Ho Song[2]

[1]*School of Chemical Engineering and Institute of Chemical Processes, Seoul National University, Seoul 151-742, Korea*
[2]*Chemical Process & Catalyst Research Center, LG Chem Research Park, LG Chemical Limited, Taejon 305-380, Korea*

Received 3 January 2002; accepted 28 May 2002

ABSTRACT: This article deals with (1) the development of a mathematical model for the finishing polycarbonate polymerization process with a horizontal, rotating disk-type reactor with countercurrent gas sweeping and (2) the performance analysis of the reactor system with the model. We propose a model describing a reactor system consisting of two phases in which the byproduct (phenol) is removed from the polymer melt phase to the countercurrently flowing vapor phase to facilitate the forward reaction and, therefore, produce a high molecular weight polymer compatible with the products of commercial grades. The vapor phase is represented by the tanks-in-series model, whereas the polymer melt phase is regarded as a plug flow reactor. The major concerns here are the influences of the reactor operating conditions, including the catalyst concentration, reaction temperature, mass-transfer rate, melt-phase residence time, and vapor-phase velocity, on the polymer molecular weight, the melt-phase concentrations of various components, and the molar fraction of phenol in the vapor phase. To corroborate the validity of the proposed model and investigate the complex phenomena of the process, we have conducted a series of simulation studies with various operating policies, and we compare the performance of the process with the performances of the cocurrent process and the vacuum process. According to the results of this study, this new type of reactor system shows satisfactory performance and is sometimes even better than the conventional high-vacuum process. © 2003 Wiley Periodicals, Inc. J Appl Polym Sci 88: 1010–1021, 2003

INTRODUCTION

Polycarbonates produced by the reaction between a carbonate ester and a diol are important engineering thermoplastics with good mechanical and optical properties as well as electrical and heat resistances useful for a number of engineering applications. Polycarbonates are usually produced in industry by interfacial polymerization and melt transesterification processes. Interfacial polymerization certainly has advantages such as efficient molecular weight control and mature process technology; however, it also suffers from serious environmental and safety problems caused by the use of toxic phosgene and organic solvents.[1] However, the melt transesterification process uses bisphenol A (BPA) and diphenyl carbonate (DPC) at a high temperature in the presence of basic catalysts such as alkali or alkaline earth metals in the form of their oxides, hydroxides, or phenolates without phosgene and solvents. Therefore, it is an environmentally benign process, and the process itself is relatively simple in comparison with the interfacial polymerization process.[2]

In the melt transesterification process, polycarbonate is produced by reversible condensation reactions in the presence of the catalyst $LiOH \cdot H_2O$; volatile species, especially phenol, should be removed from the reaction medium to facilitate the forward chain-growth reaction and to produce, therefore, a high molecular weight polymer. As the reaction proceeds, however, the viscosity of the reaction medium increases so significantly that it becomes more and more difficult to remove the byproducts and shift the equilibrium to the right. According to previous reports that dealt with a poly(ethylene terephthalate) (PET) process having features very similar to those of the polycarbonate process, the byproducts are usually removed with a horizontal disk-type reactor system under a very low pressure.[3–6] Such a vacuum process, although effective from the viewpoint of condensate removal, is costly because of the vacuum equipment and the use of high-pressure steam. Therefore, there is a demand for a more economically advantageous process with a lower cost.

Recently, an improved process for the production of polycondensation polymers has been disclosed.[7–9] A number of experimental works and theoretical studies on modeling and performance analysis for the new process have been carried out.[10–13] Nevertheless, little

Correspondence to: H.-K. Rhee (hkrhee@snu.ac.kr).
Contract grant sponsor: LG Chemical Co.
Contract grant sponsor: Brain Korea Program (supported by the Korean Ministry of Education).

Journal of Applied Polymer Science, Vol. 88, 1010–1021 (2003)

TABLE I
Reacting Species

A_n	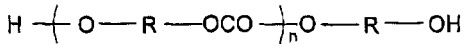
B_n	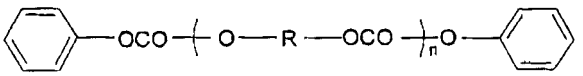
C_n	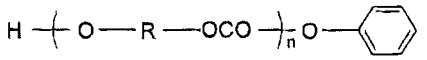
P	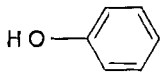
R	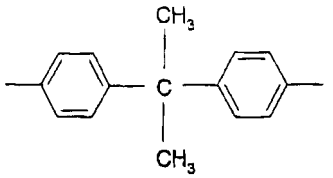

has been reported on the characteristic phenomena taking place inside the reactor system under various operating conditions.

In this study, we suggest a new approach for the modeling of the gas sweeping process using a finishing horizontal polycondensation reactor with rotating disks and doughnut-like baffles.[8] We then employ the model to analyze the performance of the countercurrent gas sweeping process. Simulation studies are carried out under conditions as close to those of industrial practice as possible. The results give us a better understanding of the gas sweeping process and provide us with useful information for the design and operation of the reactor system.

MODELING AND NUMERICAL SCHEME

The melt polycondensation of BPA and DPC is represented by the following sequence of reactions:[14]

$$A_n + B_m \underset{k'}{\overset{k}{\rightleftarrows}} C_{n+m+1} + P \quad n, m \geq 0 \tag{1}$$

$$B_n + C_m \underset{k'}{\overset{k}{\rightleftarrows}} B_{n+m} + P \quad n \geq 0, m \geq 1 \tag{2}$$

$$A_n + C_m \underset{k'}{\overset{k}{\rightleftarrows}} A_{n+m} + P \quad n \geq 0, m \geq 1 \tag{3}$$

$$C_n + C_m \underset{k'}{\overset{k}{\rightleftarrows}} C_{n+m} + P \quad n, m \geq 1 \tag{4}$$

A_n, B_n, C_n, and P are defined in Table I. In particular, A_0 and B_0 denote BPA and DPC, respectively. Also, k and k' denote the reaction rate constants of the forward and back reactions, respectively,[15] which are presented in Table II.

For the production of a high molecular weight polymer, it is important to remove phenol from the polymer melt phase to the vapor phase because the polymerization reaction for polycarbonate is reversible. Therefore, a horizontal vessel equipped with rotating disks is used to increase the interfacial area. The reactor vessel is equipped with a series of doughnut-like baffles to help the inert gas sweep over the surface of the polymer film formed on both sides of each rotating disk.[8] The basic configuration of the reactor system is depicted schematically in Figure 1(a). The inert gas flows countercurrently through the center of the baffle and toward the space between the baffle and the rotating disk. After the gas flows around the edge of the disk, it sweeps over the backside of the rotating disk and then flows toward the center of the next baffle, and so on. As the horizontal shaft rotates, on which the disks are mounted, a small amount of molten polymer is dragged upward to form a thin layer of the polymer on each rotating disk. Although the thin film is exposed to the countercurrently flowing gas, volatile species consisting mainly of the condensation byproduct, phenol, are removed from the film.

We have developed a two-phase model[16,17] consisting of the polymer melt phase and the vapor phase for this continuous finishing-stage melt polycondensation reactor system, as shown in Figure 1(b). According to Laubriet et al.,[5] the flow pattern of the polymer melt phase is properly described by the plug flow model. With the configuration of the reactor equipped with a series of rotating disks and baffles, it would be reasonable to employ the tanks-in-series model for the vapor phase. In this model, the vapor phase is properly sectionalized in such a way that each tank contains one rotating disk. This arrangement appears to be quite reasonable because the flow pattern around a rotating disk becomes repetitive along the reactor axis, and most of the condensate molecules are mass-trans-

TABLE II
Kinetic Parameters and Saturated Vapor Pressures

$$k = 4.890 \times 10^{11} \exp\left(\frac{-21{,}048}{RT}\right)[C_{cat}]\left(\frac{\text{L}}{\text{mol min}}\right)$$

$$k' = 8.180 \times 10^{9} \exp\left(\frac{-16{,}884}{RT}\right)[C_{cat}]\left(\frac{\text{L}}{\text{mol·min}}\right)$$

$$\ln P_{\text{P}}^{\text{sat}} = 16.4281 - \frac{3490.907}{T - 98.581}\ (\text{mm Hg})$$

$$\ln P_{\text{B0}}^{\text{sat}} = \left(-\frac{14.76 \times 10^3}{1.987}\right)\frac{1}{T} + 19.5521\ (\text{mmHg})$$

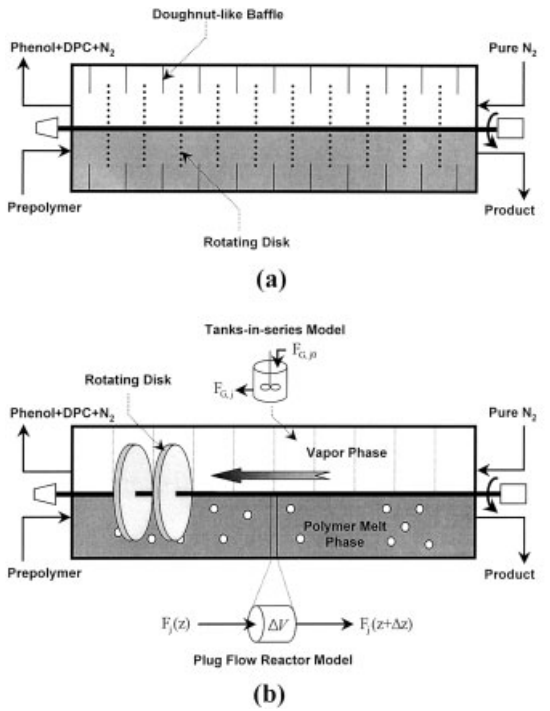

Figure 1 Schematic diagram of the gas sweeping process: (a) the reactor configuration and (b) the plug flow model for the polymer melt phase and the tanks-in-series model for the vapor phase.

ferred through the surface of the polymer film on the rotating disk; this makes the polymerization reaction most active there.

Based on reactions (1)–(4), the reaction rate expressions are formulated with the method of moments on the basis of the molecular species model, in which each chemical species is considered an independent reactive compound. In the steady state, equations for the monomer species in the polymer melt phase and for the moments of polymer concentrations are readily established as follows:

$$\frac{1}{\theta_L}\frac{d[A_0]}{dz} = k(-4[A_0][B_0] - 4[A_0]\lambda_{B,0} - 2[A_0]\lambda_{C,0}) + k'(2[P]\lambda_{A,0} + [P]\lambda_{C,0}) \quad (5)$$

$$\frac{1}{\theta_L}\frac{d[B_0]}{dz} = k(-4[A_0][B_0] - 4[B_0]\lambda_{A,0} - 2[B_0]\lambda_{C,0}) + k'(2[P]\lambda_{B,0} + [P]\lambda_{C,0}) - (k_La)_{B_0}([B_0] - [B_0]^*) \quad (6)$$

$$\frac{1}{\theta_L}\frac{d[P]}{dz} = k(4[A_0][B_0] + 4[A_0]\lambda_{B,0} + 4[B_0]\lambda_{A,0} + 4\lambda_{A,0}\lambda_{B,0} + 2[A_0]\lambda_{C,0} + 2\lambda_{A,0}\lambda_{C,0} + 2[B_0]\lambda_{C,0} + 2\lambda_{B,0}\lambda_{C,0} + (\lambda_{C,0})^2) + k'(-2[P]\lambda_{C,1} - 2[P]\lambda_{A,1} - 2[P]\lambda_{B,1} + [P]\lambda_{C,0}) - (k_La)_P([P] - [P]^*) \quad (7)$$

$$\frac{1}{\theta_L}\frac{d\lambda_{A,0}}{dz} = k(-4[B_0]\lambda_{A,0} - 4\lambda_{A,0}\lambda_{B,0} + 2[A_0]\lambda_{C,0}) + k'([P]\lambda_{C,1} - [P]\lambda_{C,0} - 2[P]\lambda_{A,0}) \quad (8)$$

$$\frac{1}{\theta_L}\frac{d\lambda_{A,1}}{dz} = k(-4[B_0]\lambda_{A,1} - 4\lambda_{A,1}\lambda_{B,0} + 2[A_0]\lambda_{C,1} + 2\lambda_{A,0}\lambda_{C,1}) + k'\left(\frac{1}{2}[P]\lambda_{C,2} - \frac{1}{2}[P]\lambda_{C,1} - [P]\lambda_{A,2} - [P]\lambda_{A,1}\right) \quad (9)$$

$$\frac{1}{\theta_L}\frac{d\lambda_{A,2}}{dz} = k(-4[B_0]\lambda_{A,2} - 4\lambda_{A,2}\lambda_{B,0} + 2[A_0]\lambda_{C,2} + 4\lambda_{A,1}\lambda_{C,1} + 2\lambda_{A,0}\lambda_{C,2}) + k'\left(\frac{1}{3}[P]\lambda_{C,3} - \frac{1}{2}[P]\lambda_{C,2} + \frac{1}{6}[P]\lambda_{C,1} - \frac{4}{3}[P]\lambda_{A,3} - [P]\lambda_{A,2} + \frac{1}{3}[P]\lambda_{A,1}\right) \quad (10)$$

$$\frac{1}{\theta_L}\frac{d\lambda_{B,0}}{dz} = k(-4[A_0]\lambda_{B,0} - 4\lambda_{A,0}\lambda_{B,0} + 2[B_0]\lambda_{C,0}) + k'([P]\lambda_{C,1} - [P]\lambda_{C,0} - 2[P]\lambda_{B,0}) \quad (11)$$

$$\frac{1}{\theta_L}\frac{d\lambda_{B,1}}{dz} = k(-4[A_0]\lambda_{B,1} - 4\lambda_{B,1}\lambda_{A,0} + 2[B_0]\lambda_{C,1} + 2\lambda_{B,0}\lambda_{C,1}) + k'\left(\frac{1}{2}[P]\lambda_{C,2} - \frac{1}{2}[P]\lambda_{C,1} - [P]\lambda_{B,2} - [P]\lambda_{B,1}\right) \quad (12)$$

$$\frac{1}{\theta_L}\frac{d\lambda_{B,2}}{dz} = k(-4[A_0]\lambda_{B,2} - 4\lambda_{B,2}\lambda_{A,0} + 2[B_0]\lambda_{C,2} + 4\lambda_{B,1}\lambda_{C,1} + 2\lambda_{B,0}\lambda_{C,2}) + k'\left(\frac{1}{3}[P]\lambda_{C,3} - \frac{1}{2}[P]\lambda_{C,2} + \frac{1}{6}[P]\lambda_{C,1} - \frac{4}{3}[P]\lambda_{B,3} - [P]\lambda_{B,2} + \frac{1}{3}[P]\lambda_{B,1}\right) \quad (13)$$

$$\frac{1}{\theta_L}\frac{d\lambda_{C,0}}{dz} = k\{4[A_0][B_0] + 4[A_0]\lambda_{B,0} + 4[B_0]\lambda_{A,0} + 4\lambda_{A,0}\lambda_{B,0} - 2[A_0]\lambda_{C,0} - 2\lambda_{A,0}\lambda_{C,0} - 2[B_0]\lambda_{C,0} - 2\lambda_{B,0}\lambda_{C,0} - (\lambda_{C,0})^2\} + k'(-[P]\lambda_{C,0} + 2[P]\lambda_{A,1} + 2[P]\lambda_{B,1}) \quad (14)$$

$$\frac{1}{\theta_L}\frac{d\lambda_{C,1}}{dz} = k(4[A_0][B_0] + 4[A_0]\lambda_{B,1} + 4[A_0]\lambda_{B,0} + 4[B_0]\lambda_{A,0} + 4[B_0]\lambda_{A,1} + 4\lambda_{A,1}\lambda_{B,0} + 4\lambda_{A,0}\lambda_{B,1} + 4\lambda_{A,0}\lambda_{B,0} - 2[A_0]\lambda_{C,1} - 2\lambda_{A,0}\lambda_{C,1} - 2[B_0]\lambda_{C,1} - 2\lambda_{B,0}\lambda_{C,1}) + k'([P]\lambda_{B,1} - [P]\lambda_{C,2} + [P]\lambda_{A,1} + [P]\lambda_{B,2} + [P]\lambda_{A,2}) \quad (15)$$

TABLE III
Reactor Dimensions and Standard Operating Conditions

Reactor dimension		Standard operating condition	
Total volume	5.114 L	Total pressure	1 atm
Melt-phase volume	1.704 L	Reaction temperature	280°C
Number of disks	10	Melt-phase residence time	90 min
Reactor length	55 cm	Superficial velocity of the vapor phase	20 cm/s
Outer diameter of the rotating disk	10 cm	Amount of catalyst ($LiOH \cdot H_2O$)	0.005 wt %
Inner diameter of the rotating disk	5 cm	$(k_La)_P$	2.0 min^{-1}

$$\frac{1}{\theta_L}\frac{d\lambda_{C,2}}{dz} = k\{4[A_0][B_0] + 4[A_0]\lambda_{B,2} + 8[A_0]\lambda_{B,1} + 4[A_0]\lambda_{B,0} + 4[B_0]\lambda_{A,2} + 4\lambda_{A,2}\lambda_{B,0} + 8[B_0]\lambda_{A,1} + 8\lambda_{A,1}\lambda_{B,1} + 8\lambda_{A,1}\lambda_{B,0} + 4[B_0]\lambda_{A,0} + 4\lambda_{A,0}\lambda_{B,2} + 8\lambda_{A,0}\lambda_{B,1} + 4\lambda_{A,0}\lambda_{B,0} - 2[A_0]\lambda_{C,2} - 2\lambda_{A,0}\lambda_{C,2} - 2[B_0]\lambda_{C,2} - 2\lambda_{B,0}\lambda_{C,2} + 2(\lambda_{C,1})^2\} + k'\left(\frac{2}{3}[P]\lambda_{A,3} + [P]\lambda_{A,2} + \frac{1}{3}[P]\lambda_{A,1} + \frac{2}{3}[P]\lambda_{B,3} + [P]\lambda_{B,2} + \frac{1}{3}[P]\lambda_{B,1} - \frac{4}{3}[P]\lambda_{C,3} + \frac{1}{3}[P]\lambda_{C,1}\right) \quad (16)$$

$\lambda_{\xi,\chi}$ is the χth moment of the polymer concentrations, where ξ represents the type of polymeric species. Also, θ_L, z, $[C_j]$, $[C_j]^*$, k_L, and a denote the melt-phase residence time, the dimensionless axial distance along the flow of the polymer melt phase, the concentration of species j in the polymer melt phase, the equilibrium concentration of species j at the interface, the mass-transfer coefficient, and the specific interfacial area, respectively. The third moment of the polymer concentrations is calculated with the moment closure technique.[18]

It is then possible to determine the average molecular weights and polydispersity index (PDI) with the moment equations as follows:

$$M_n = \frac{\sum_{n=1}^{\infty}\{[A_n](254.3n + 228.29) + [B_n](254.3n + 214.22) + [C_n](254.3n + 94.11)\}}{\sum_{n=1}^{\infty}([A_n] + [B_n] + [C_n])} = \frac{\mu_1}{\mu_0} \quad (17)$$

$$M_w = \frac{\sum_{n=1}^{\infty}\{[A_n](254.3n + 228.29)^2 + [B_n](254.3n + 214.22)^2 + [C_n](254.3n + 94.11)^2\}}{\sum_{n=1}^{\infty}\{[A_n](254.3n + 228.29) + [B_n](254.3n + 214.22) + [C_n](254.3n + 94.11)\}} = \frac{\mu_2}{\mu_1} \quad (18)$$

$$\text{PDI} = \frac{M_w}{M_n} \quad (19)$$

where M_n and M_w are the number-average and weight-average molecular weights, respectively, and μ_0, μ_1, and μ_2 are given by

$$\mu_0 = \lambda_{A,0} + \lambda_{B,0} + \lambda_{C,0} \quad (20)$$

$$\mu_1 = 254.3(\lambda_{A,1} + \lambda_{B,1} + \lambda_{C,1}) + 228.29\lambda_{A,0} + 214.22\lambda_{B,0} + 94.11\lambda_{C,0} \quad (21)$$

$$\mu_2 = (254.3)^2(\lambda_{A,2} + \lambda_{B,2} + \lambda_{C,2}) + 2(254.3)(228.29\lambda_{A,1} + 214.22\lambda_{B,1} + 94.11\lambda_{C,1}] + (228.29)^2\lambda_{A,0} + (214.22)^2\lambda_{B,0} + (94.11)^2\lambda_{C,0} \quad (22)$$

We are now in a position to derive the equations for the molar fraction of the volatile species j in the vapor phase. It is assumed that only phenol and DPC vaporize because BPA is much less volatile than phenol and DPC[19,20] and that no reaction takes place in the vapor phase. We have adopted here the two-phase model[16,17] and assumed that there is no mass-transfer resistance in the vapor phase. For a typical tank, among the series of tanks for the vapor phase, the mass-balance equation for the volatile species j in the vapor phase can be written as follows:

$$q[C_j]_{G,\text{out}} = q[C_j]_{G,\text{in}} + \int_{z_{\text{in}}}^{z_{\text{out}}}\{(k_La)_j([C_j] - [C_j]^*)S\}dz \quad (j = \text{phenol and DPC}) \quad (23)$$

where q, $[C_j]_{G,\text{in}}$ and $[C_j]_{G,\text{out}}$, z_{in} and z_{out}, and S denote the volumetric flow rate of the vapor phase, the concentrations of species j at the inlet and outlet of the tank, the starting and end points of the tank along the reactor axis in the direction of the gas flow, and the cross-sectional area of the polymer melt phase, respectively. Because $[C_j]$ and $[C_j]^*$ represent the concentrations per unit volume of the polymer, the integration is performed over the volume of the polymer melt phase. Therefore, eq. (23) may be rearranged to give

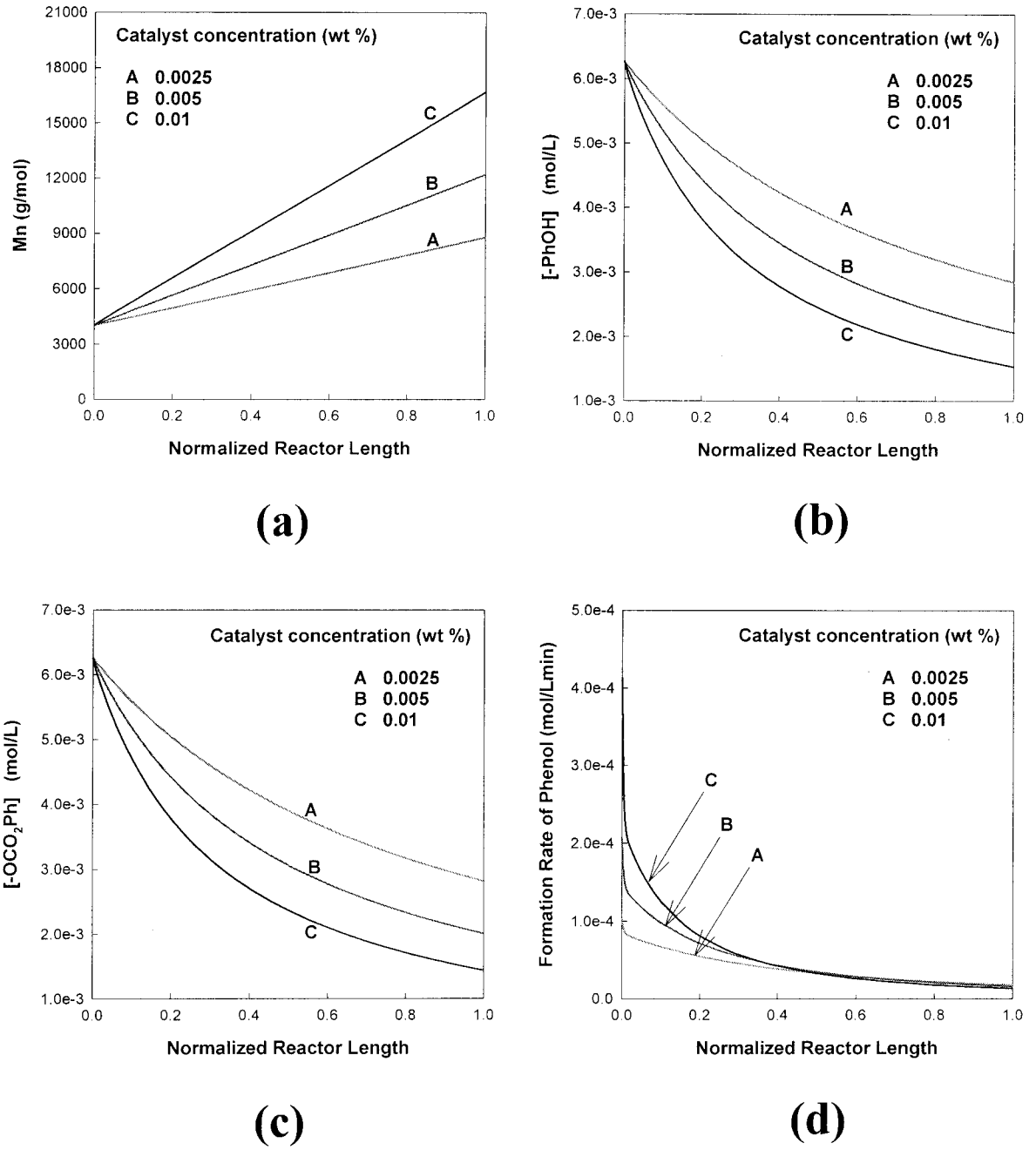

Figure 2 Performance of the reactor system for three different values of the catalyst concentration: (a) M_n, (b) the concentration of the hydroxyl end groups, (c) the concentration of the phenyl carbonate end groups, and (d) the formation rate of phenol.

$$[C_j]_{G,out} = [C_j]_{G,in} + \frac{\theta_G}{V_G}\int_{z_{in}}^{z_{out}} \{(k_L a)_j([C_j] - [C_j]^*)S\}dz \tag{24}$$

where θ_G and V_G denote the vapor-phase residence time and the volume of the vapor phase for the tank, respectively. If we include the concentration of nitrogen in the tank ($[N_2]_G$), which may be calculated by the ideal gas law, the molar fraction of the volatile species j in the tank is given by

$$y_j = \frac{[C_j]_{G,out}}{\sum_j ([C_j]_{G,out}) + [N_2]_G} \tag{25}$$

With the reactor model developed here, a series of simulation studies have been conducted to investigate

the behavior of the reactor system. The standard value of k_La for phenol has been adopted from the literature,[12] whereas that of DPC has been calculated with the proportionality property of k_La with respect to the saturated vapor pressure[21] as follows:

$$(k_La)_{B0} = (k_La)_P \times \frac{P_{B0}^{sat}}{P_P^{sat}} \quad (26)$$

where P_{B0}^{sat} and P_P^{sat} denote the saturated vapor pressures of DPC and phenol, respectively. The saturated vapor pressure data[19] used in this study are found in Table II. The equilibrium concentration of the volatile species j at the interface is calculated by the following equation:

$$[C_j]^* = \left(\frac{[C_{poly}]}{1 - \sum_j x_j^*}\right) x_j^* \quad (j = \text{phenol and DPC}) \quad (27)$$

where $[C_{poly}]$ and x_j^* denote the total concentration of the polymeric species and the equilibrium molar fraction of volatile species j in the polymer melt phase,[22] respectively. That is,

$$[C_{poly}] = \lambda_{A,0} + \lambda_{B,0} + \lambda_{C,0} \quad (28)$$

$$x_j^* = \frac{P_t y_j}{P_j^{sat} \gamma_j} \quad (29)$$

P_t represents the total pressure, and the Flory–Huggins equation[23] is employed to calculate the activity coefficient γ_j.

The molar fraction of species j in the vapor phase is calculated as follows. First, the respective vapor-phase molar fractions of phenol and DPC are specified. Then, the interfacial molar concentrations and the molar concentrations of polymeric species in the polymer melt phase are calculated by eqs. (5)–(16) and eqs. (27)–(29) together with the Flory–Huggins equation. The vapor-phase molar fractions of the volatile species are then revised from the last tank to the first one with the resulting concentrations and eq. (25). This procedure is repeated until the changes in the molar fractions from the previous step become smaller than prescribed criteria.

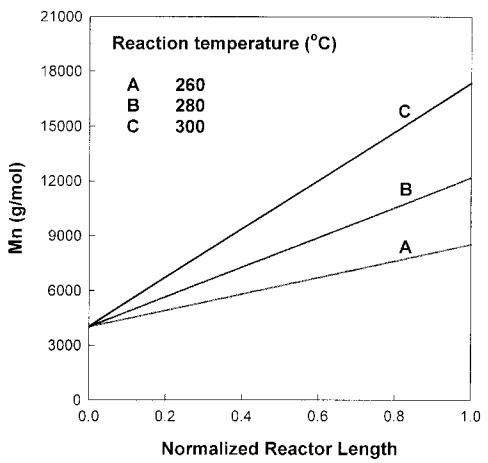

Figure 3 Profiles of M_n for three different values of the reaction temperature.

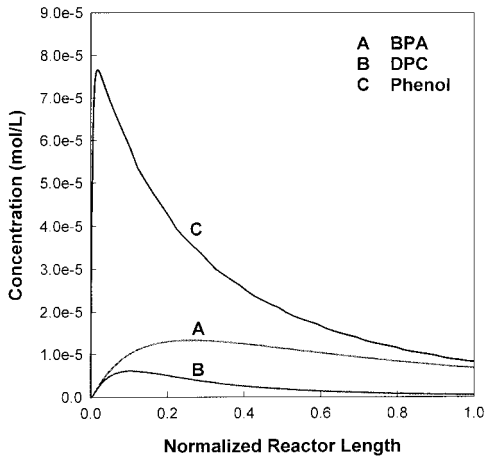

Figure 4 Profiles of the concentrations of BPA, DPC, and phenol in the polymer melt phase under the standard operating conditions.

RESULTS AND DISCUSSION

The operating conditions showing a significant influence on the performance of the finishing reactor are the catalyst concentration, the reaction temperature, and the residence times of the polymer melt phase and vapor phase. In addition, the k_La value for each volatile species is expected to be an important factor affecting the polymer properties. The reactor is operated by the regulation of these operating conditions in such a way that a desired degree of polymerization is obtained. Therefore, it is of practical interest to investigate how the polymer molecular weight, the molar fraction of phenol in the vapor phase, and the concentrations of functional end groups and individual components in the polymer melt phase may change with the variations in one or more of the reactor operating conditions. The reactor dimensions and standard operating conditions for the simulation study are summarized in Table III.

The prepolymer feed to the finishing disk-type polycondensation reactor has a low molecular weight and consists of equal amounts of functional end groups, [—PhOH] (hydroxyl end groups) and [—OCO_2Ph] (phenyl carbonate end groups), produced in the prior semibatch reactor. M_n of this prepolymer feed is about 4000, and the corresponding degree of polymerization is 16.

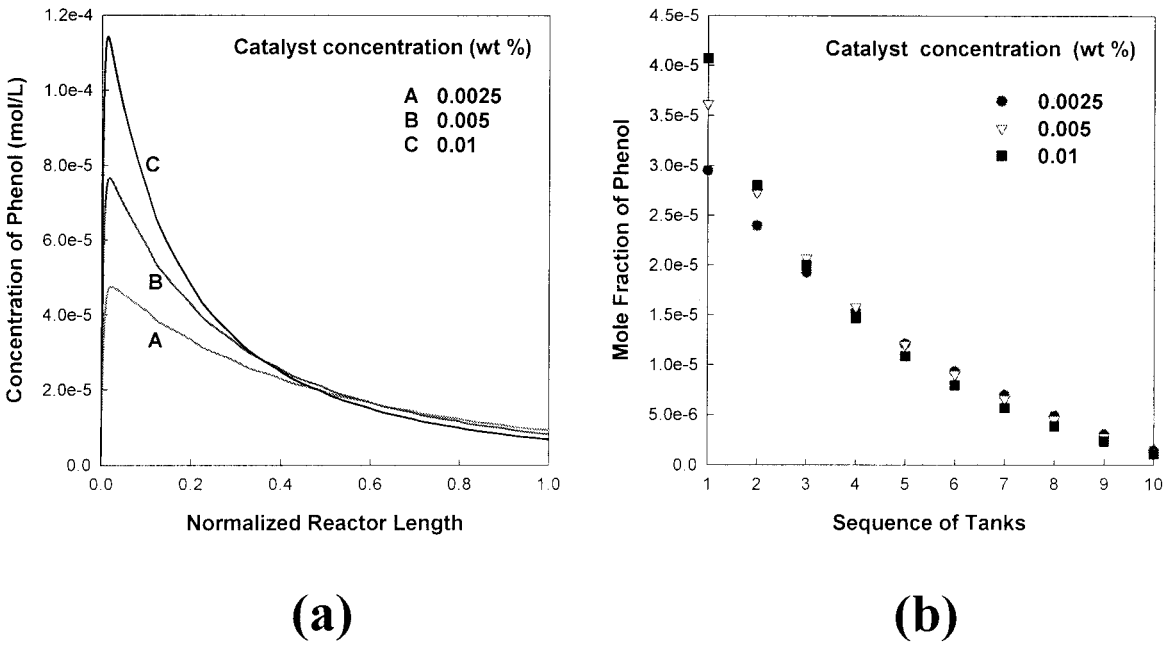

Figure 5 Effect of the catalyst concentration on the steady-state behavior of the polycarbonate polymerization process with gas sweeping: (a) the concentration of phenol in the polymer melt phase and (b) the molar fraction of phenol in the vapor phase.

Under the standard operating conditions, M_n at the exit of the reactor is 12,200, which is in good agreement with the experimental results reported in the literature.[11–13] Although the method of gas sweeping treated in the literature is different from ours, it seems reasonable to make the comparison because the inert gas sweeping is used under similar reaction conditions in both cases. According to the results of the simulation study, the PDI remains nearly constant at about 1.9 during the entire course of the reaction.

Effects of the catalyst concentration and reaction temperature

As shown in Figure 2(a), M_n increases with the catalyst concentration. The molecular weight increases almost linearly along the reactor axis, and this trend agrees well with the experimental results reported in the patent related to the gas sweeping process[9] and also with other simulation results for the PET polymerization process,[10] the characteristics of which are similar to those of the polycarbonate polymerization process. Figure 2(b,c) shows that the concentrations of the functional end groups ([—PhOH] and [—OCO_2Ph]) become fairly large at the reactor inlet. According to reactions (1)–(4), such large concentrations would give rise to a fast rate of polymerization and a rapid increase in the amount of phenol formed. As the polymer melt phase flows toward the reactor outlet, the concentrations of the functional end groups tend to decrease rapidly, and this results in a decrease in the production rate of phenol, as illustrated in Figure 2(d). When the flow of the polymer melt phase proceeds to about 40% of the reactor length, the concentrations of the functional end groups are reduced by about 50%, and this indicates that the rate of reaction can be reduced to about a quarter of the rate at the inlet. This also agrees well with a previous report in the literature.[6]

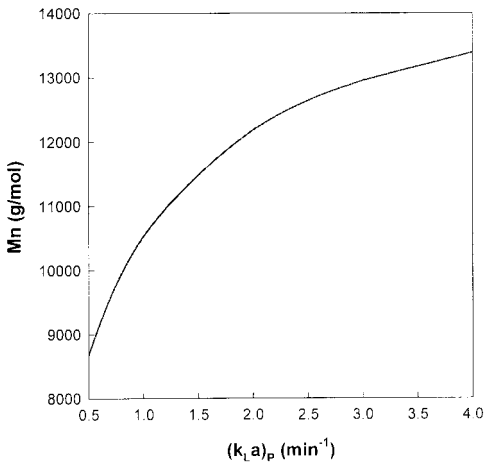

Figure 6 Effect of $(k_La)_P$ on M_n at the reactor exit in the steady state.

This phenomenon would remain nearly the same in the conventional vacuum process,[3–6] and so the increasing rate of the molecular weight would slow down. In the countercurrent process with the inert gas flow from the end of the reactor, however, the sweeping gas makes a larger driving force for mass transfer, especially near the reactor exit, than that in the vacuum process and, therefore, enhances the mass-transfer rate of volatile species. As a result, the increasing rate of the molecular weight can be maintained even

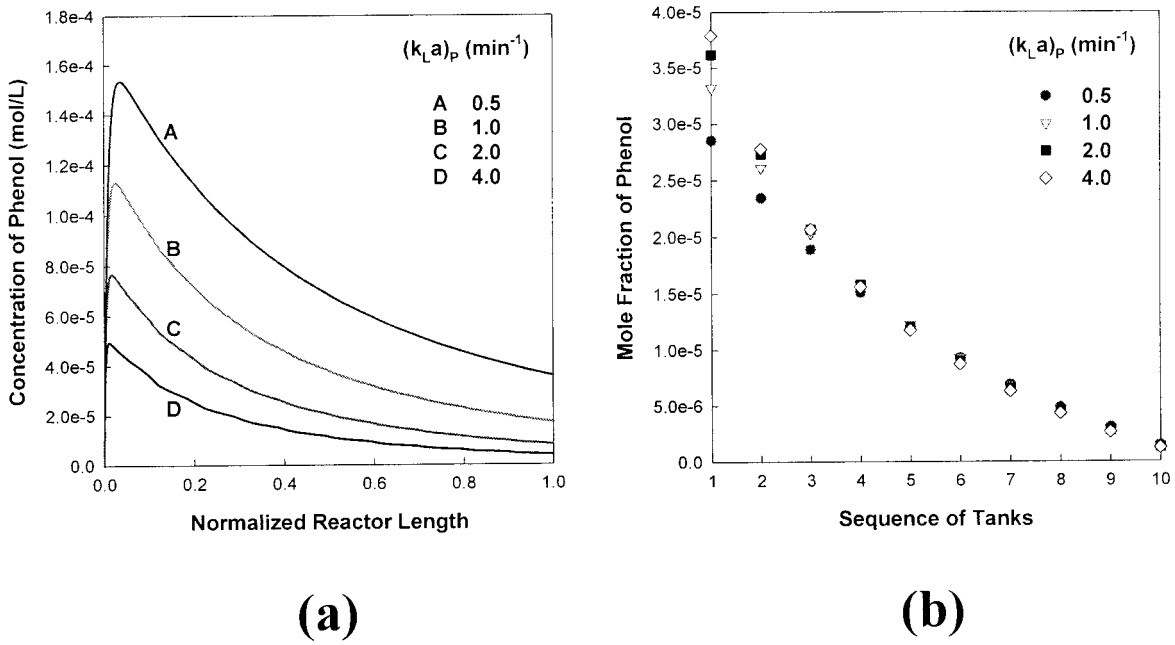

Figure 7 Effect of $(k_La)_P$ on the steady-state behavior of the polycarbonate polymerization process with gas sweeping: (a) the concentration of phenol in the polymer melt phase and (b) the molar fraction of phenol in the vapor phase.

to the reactor exit, and so the molecular weight increases almost linearly over the entire length of the reactor. The results of simulation studies at different reaction temperatures are presented in Figure 3. Because the rate of reaction has a strong dependence on the reaction temperature, the increasing rate of the molecular weight is rather large.

The composition of volatile species in the prepolymer feed is set equal to zero in our simulation study. According to reactions (1)–(4), phenol is produced rapidly near the reactor inlet, and this is shown in Figure 4. After the peak near the reactor inlet, the concentration decreases steadily because of the mass transfer from the polymer melt phase to the vapor phase as well as the decrease in the rate of formation of phenol caused by the decrease in the amount of the reacting species [cf. Fig. 2(d)].

Figure 5(a,b) shows the concentrations of phenol in the polymer melt phase and vapor phase for three different values of the catalyst concentration. As discussed earlier, the higher the catalyst concentration is near the reactor inlet, the more vigorously the polycondensation reaction proceeds, and so the molar concentration of phenol in the polymer melt phase becomes high. Beyond about 40% of the reactor length, however, as the catalyst concentration increases, the polycondensation reaction slows down more rapidly because of the faster consumption of the polymeric species in the upstream side, and so the concentration of phenol in the polymer melt phase becomes lower. The effects of the reaction temperature on the concentrations of phenol in both phases are similar, although the reaction temperature exercises a more significant influence than the catalyst concentration.

Effect of k_La

Another factor affecting the molecular weight significantly is the mass-transfer rate of volatile species. The $(k_La)_P$ value reported in the literature[12] ranges from 0.5 to 4.0 min^{-1} as the reaction temperature changes from 260 to 300°C. Although the type of reactor system is somewhat different from ours, we presume that the order of magnitude of the $(k_La)_P$ value would be the same, and we use values of 0.5–4.0 min^{-1} for our simulation study to examine the effect of k_La on the performance of the reactor system. Because the reaction is reversible and the removal of the condensate, phenol, certainly facilitates the forward reaction, the molecular weight increases with $(k_La)_P$, as shown in Figure 6. As $(k_La)_P$ becomes large, its effect tends to become weak.

In Figure 7, we present the profiles of the concentration of phenol in the polymer melt phase and the molar fraction of phenol in the vapor phase for four different values of $(k_La)_P$. With a large value of $(k_La)_P$, phenol is removed more efficiently from the polymer melt phase. Therefore, the concentration of phenol in the polymer melt phase becomes lower, and the forward reaction is facilitated. Beyond the peak point of the concentration profile, however, the rapid consumption of the polymeric species in the upstream side reduces the rate of production for phenol in the polymer melt phase and, therefore, the amount of

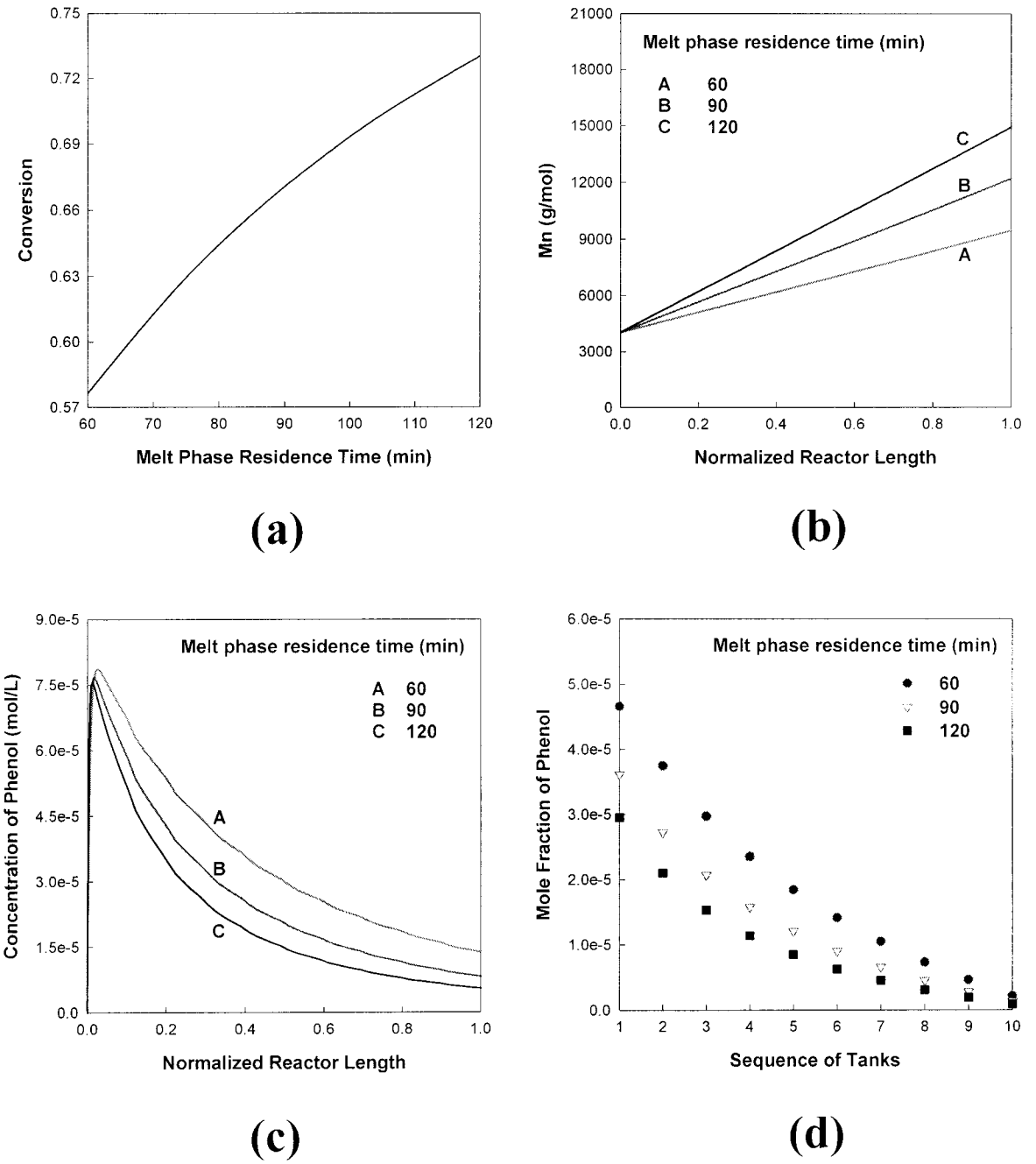

Figure 8 Effect of the melt-phase residence time on the steady-state behavior of the polycarbonate polymerization process with gas sweeping: (a) the conversion, (b) M_n, (c) the concentration of phenol in the polymer melt phase, and (d) the molar fraction of phenol in the vapor phase.

phenol mass-transferred to the vapor phase. As shown in Figure 7(b), the molar fraction of phenol in the upstream side of the inert gas becomes lower when $(k_L a)_P$ is larger.

Effect of the melt-phase residence time

Figure 8 presents the effect of the residence time of the polymer melt phase. As the melt-phase residence time increases, the contact time between the polymer film on the rotating disk and the countercurrently flowing gas increases. As a result, the conversion and, therefore, M_n increase with the melt-phase residence time, as shown in Figure 8(a,b). In Figure 8(c,d), we present the molar concentration of phenol in the polymer melt phase and the molar fraction of phenol in the vapor phase for three different values of the melt-phase residence time. The shorter melt-phase residence time or the faster feed rate leads to an increase in the concentration of phenol in both phases.

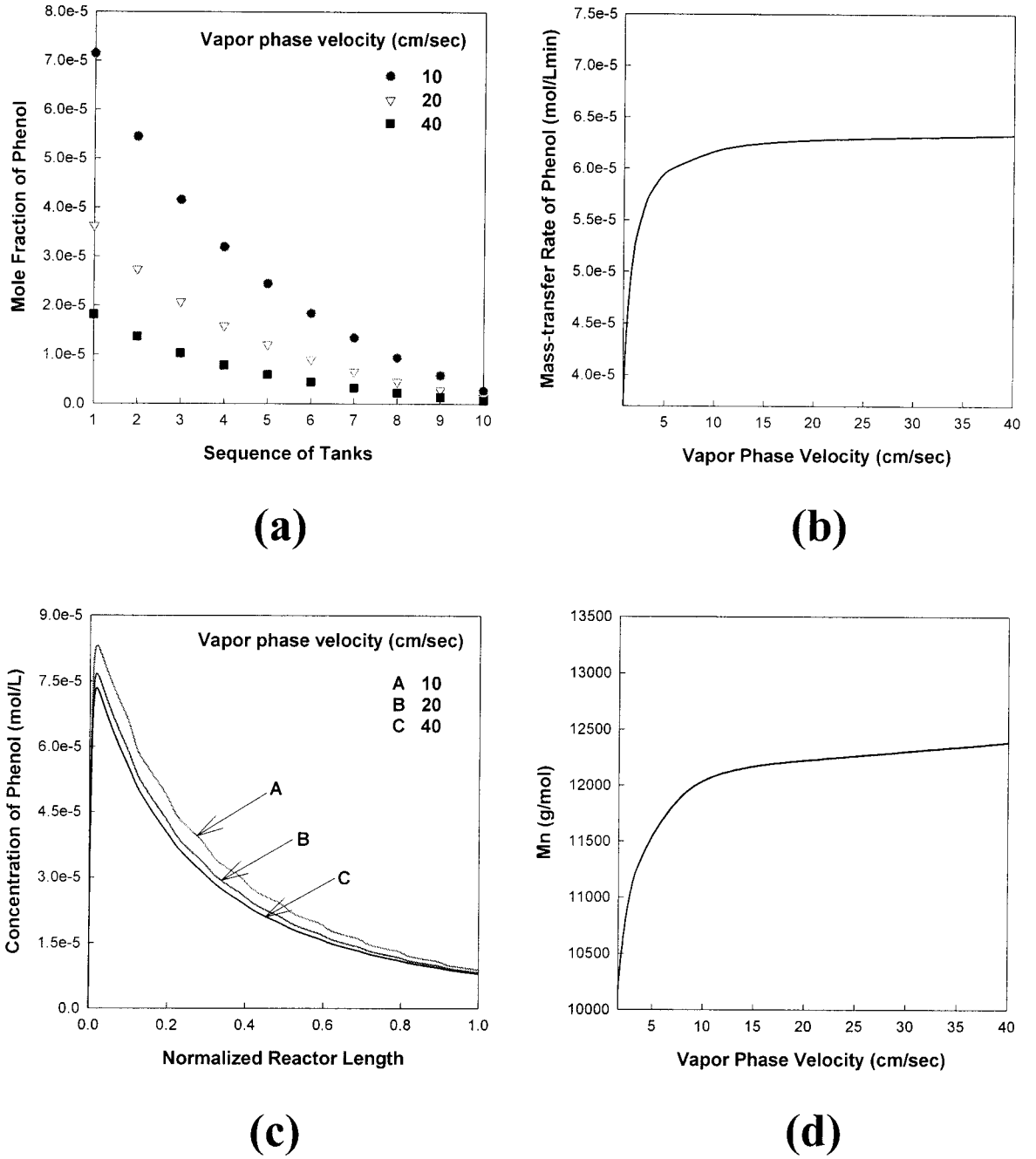

Figure 9 Effect of the vapor-phase velocity on the steady-state behavior of the polycarbonate polymerization process with gas sweeping: (a) the molar fraction of phenol in the vapor phase, (b) the mass-transfer rate of phenol from the polymer melt phase to the vapor phase, (c) the concentration of phenol in the polymer melt phase, and (d) M_n at the reactor exit.

Effect of the gas sweeping rate on the vapor phase

Figure 9 shows the effect of the vapor-phase velocity, which is based on the empty cross section of the reactor. The effect of the gas sweeping is strengthened with the faster vapor-phase velocity, which keeps the molar fraction in the vapor phase low, as shown in Figure 9(a). Figure 9(b,c) presents the mass-transfer rate of phenol at the position 25% downstream of the reactor length for various gas sweeping rates and the molar concentration of phenol in the polymer melt phase for three different values of the vapor-phase velocity, respectively. The reduced molar fraction facilitates the mass transfer, so the concentration of phenol in the polymer melt phase also decreases. Therefore, the forward reaction is facilitated and the higher molecular weight is obtained with the faster vapor-phase velocity, as shown in Figure 9(d).

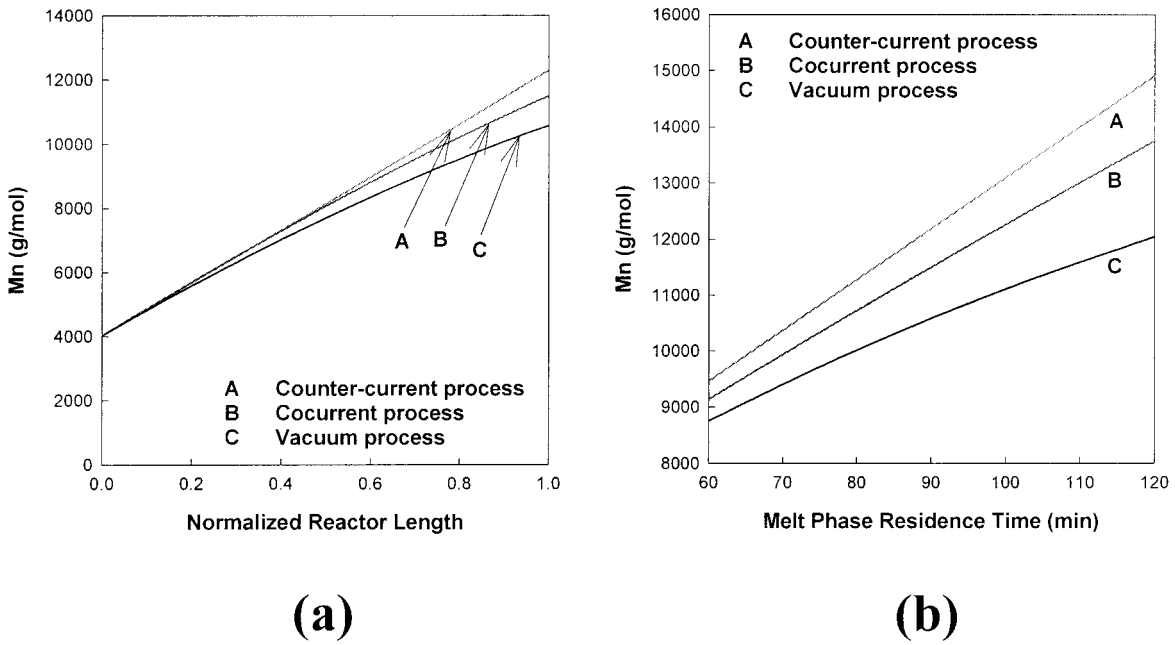

Figure 10 Comparison of the reactor performances for three different types of reactor operations under the same standard operating conditions: (a) profiles of M_n and (b) effects of the melt-phase residence time.

Another feature to be noticed is that the effect of the vapor-phase velocity is rather limited and beyond a certain critical value, its influence becomes really insignificant. Under this circumstance, the excessively fast vapor-phase velocity would simply bring about a high cost to reflux the inert gas. This observation is in good agreement with the discussion in the patent related to the gas sweeping process.[9]

Comparison of the countercurrent and cocurrent processes and the vacuum process

In Figure 10(a), the reactor performances are compared for three different types of reactor operations, that is, the countercurrent and cocurrent gas sweeping processes and the vacuum process under the standard operating conditions listed in Table III. The pressure for the vacuum process is set equal to 0.05 mmHg. Clearly, the countercurrent process is superior to the other two processes, and the advantage becomes more distinct as the residence time of the polymer melt phase increases, as shown in Figure 10(b). This indicates that the countercurrent gas sweeping process has potential as an alternative to the conventional high-vacuum process.

CONCLUSIONS

A mathematical model has been developed for a finishing melt polycondensation reactor with countercurrent gas sweeping, and it has been used for simulation studies to demonstrate that the polymer molecular weight can be effectively increased within a reasonable range of residence times in the production of polycarbonate. One of the advantages of this process is that the condensate, phenol, can be easily removed from the highly viscous polymer melt with a countercurrently sweeping gas over the polymer melt phase at the ambient pressure.

An increase in the catalyst concentration or in the reaction temperature directly gives rise to an increase in both forward and back reaction rates, whereas an increase in the k_La value for the condensate promotes the forward reaction significantly. Nevertheless, all of these three cases lead to an increase in the average molecular weights. A longer residence time of the polymer melt phase increases both the conversion and the molecular weight, but the productivity per unit time decreases because of the low flow rate of the polymer melt phase. In contrast, a shorter residence time of the vapor phase increases the conversion, molecular weight, and productivity by virtue of the facilitated removal of the condensate. However, there exists an upper bound of the reactor performance if the vapor-phase velocity is the only variable to be adjusted.

It has also been shown by simulation studies that the gas sweeping process may produce polycarbonates compatible with commercial grades. In addition, this new type of reactor system presents satisfactory performance and is sometimes even better than the conventional high-vacuum process. Consequently, the gas sweeping process appears to have potential as an alternative to the conventional high-vacuum process.

NOMENCLATURE

Symbols

a	specific interfacial area (cm^2/cm^3)
$[C_j]$	molar concentration of component j (mol/L)
k and k'	forward and back reaction rate constants (L/mol min)
k_L	mass-transfer coefficient (cm/min)
M_n	number-average molecular weight (g/mol)
M_w	weight-average molecular weight (g/mol)
P	pressure (mmHg)
PDI	polydispersity index
q	volumetric flow rate of the vapor phase (L/min)
R	gas constant (cal/mol K)
S	cross-sectional area of the polymer melt phase (cm^2)
V	volume (L)
x_j	molar fraction of volatile species j in the polymer melt phase
y_j	molar fraction of volatile species j in the vapor phase
z	dimensionless distance from the reactor inlet

Greek characters

γ	activity coefficient
$\lambda_{\xi,\chi}$	χth moment of the molar concentrations of polymeric species ξ (mol/L)
$\mu 0$	defined by eq. (20) (mol/L)
$\mu 1$	defined by eq. (21) (g/L)
$\mu 2$	defined by eq. (22) (g^2/L^2)
θ	mean residence time (min)

Superscripts

*	equilibrium
sat	saturation

Subscripts

B0	DPC
cat	catalyst
G	vapor phase
in	inlet
L	polymer melt phase
P	phenol
poly	polymeric species
out	outlet
t	total

References

1. Mills, P. L. Chem Eng Sci 1986, 41, 2939.
2. Legrand, D. G.; Bendler, J. T. Handbook of Polycarbonate Science and Technology, 1st ed.; Marcel Dekker: New York, 2000.
3. Ravindranath, K.; Mashelkar, R. A. Polym Eng Sci 1982, 22, 628.
4. Ravindranath, K.; Mashelkar, R. A. AIChE J 1984, 30, 415.
5. Laubriet, C.; LeCorre, B.; Choi, K. Y. Ind Eng Chem Res 1991, 30, 2.
6. Castres Saint Martin, H.; Choi, K. Y. Ind Eng Chem Res 1991, 30, 1712.
7. Bhatia, K. K. U.S. Pat. 5,434,239 (1995).
8. Bhatia, K. K. U.S. Pat. 5,552,513 (1996).
9. Bhatia, K. K. U.S. Pat. 5,856,423 (1999).
10. Yao, Z.; Ray, W. H. AIChE J 2001, 47, 401.
11. Woo, B. G.; Choi, K. Y.; Song, K. H. Ind Eng Chem Res 2001, 40, 1312.
12. Woo, B. G.; Choi, K. Y.; Song, K. H. Ind Eng Chem Res 2001, 40, 3459.
13. Song, K. H.; Lee, S. H.; Park, K. H. Kor. Pat. 1999-73161 (1999).
14. Kim, Y. S.; Choi, K. Y. Ind Eng Chem Res 1992, 31, 2118.
15. Hersh, S. N.; Choi, K. Y. J Appl Polym Sci 1990, 41, 1033.
16. Sherwood, T. K.; Pigford, R. L.; Wilke, C. R. Mass Transfer; McGraw-Hill: New York, 1975.
17. Treybal, R. E. Mass Transfer Operation, 3rd ed.; McGraw-Hill: Singapore, 1980.
18. Tai, K.; Arai, Y.; Teranishi, H.; Tagawa, T. J Appl Polym Sci 1980, 25, 1789.
19. Kim, Y. S.; Choi, K. Y. J Appl Polym Sci 1993, 49, 747.
20. Woo, B. G.; Choi, K. Y.; Song, K. H.; Lee, S. H. J Appl Polym Sci 2001, 80, 1253.
21. Kim, Y. S. Korean J Chem Eng 1998, 15, 671.
22. Smith, J. M.; Van Ness, H. C.; Abbott, M. M. Introduction to Chemical Engineering Thermodynamics, 5th ed.; McGraw-Hill: New York, 1996.
23. Prausnitz, J. M.; Lichtenthaler, R. N.; de Azevedo, E. G. Molecular Thermodynamics of Fluid Phase Equilibria, 3rd ed.; Prentice Hall: Upper Saddle River, NJ, 1999.